

INVITED PAPER

https://doi.org/10.1070/QEL16707

Aperiodic reflection diffraction gratings for soft X-ray radiation and their application

E.A. Vishnyakov, A.O. Kolesnikov, A.S. Pirozhkov, E.N. Ragozin, A.N. Shatokhin

Contents

Abstract. **We briefly review the works concerned with the development and experimental use of the spectral instruments based on aperiodic reflection gratings whose spacing varies monotonically across the aperture according to a prescribed law (VLS gratings). The review considers the employment of VLS-grating instruments intended for the spectroscopy of laboratory and astrophysical plasmas, including the diagnostics of relativistic laser plasmas, for measuring X-ray laser linewidths, for recording the high-order harmonics of laser radiation, the radiation of fast electric discharges and other laboratory X-ray sources, as well as in reflectometry, X-ray fluorescence analysis and microscopy with the use of synchrotron radiation and laser-plasma radiation, and in emission spectroscopy combined with an electron microscope. Also discussed are achievements in the recently undertaken design and development of special-purpose VLS spectrometers intended for the investigation of the electronic structure of different materials and molecules by the spectroscopic technique of resonant inelastic X-ray scattering of synchrotron radiation. We describe flat-field grazing-incidence spectrometers with concave VLS gratings, which are compatible with modern CCD detectors, as well as plane VLS gratings, which are the key elements of scanning high- and ultrahigh-resolution spectrometers/monochromators with a constant deviation angle and stigmatic (imaging) spectrometers, which are also compatible with CCD detectors.**

Keywords: *soft X-ray/VUV radiation, VLS grating, flat-field spectrometer, stigmatic (imaging) spectrometer.*

E.A. Vishnyakov, E.N. Ragozin P.N. Lebedev Physical Institute, Russian Academy of Sciences, Leninsky prosp. 53, 119991 Moscow, Russia; e-mail: enragozin@gmail.com;
A.O. Kolesnikov, A.N. Shatokhin P.N. Lebedev Physical Institute, Russian Academy of Sciences, Leninsky prosp. 53, 119991 Moscow, Russia; Moscow Institute of Physics and Technology (State University), Institutskii per. 9, 141701 Dolgoprudnyi, Moscow region, Russia;
A.S. Pirozhkov Kansai Photon Science Institute, National Institutes for Radiological Science and Technology, 8-1-7 Umemidai, Kizugawa-city, Kyoto, 619-0215, Japan

Received 18 April 2018; revision received 16 August 2018
Kvantovaya Elektronika **48** (10) 916–929 (2018)
Translated by E.N. Ragozin

1. Introduction. Historical background

In 1882 H.A. Rowland conceived the idea of combining the dispersive properties of a classical plane diffraction grating (DG) with the focusing property of a concave mirror. He showed that a concave grating had a remarkable property: if it is placed tangentially to a circle of radius equal to half the grating radius, the spectrum of a point source lying on the circle will be focused on this circle. This circle is known as the Rowland circle, this 'source–grating' configuration received the name Rowland scheme and formed the basis for the majority of vacuum spectrographs [1, 2]. The transition to spectrographs with grazing radiation incidence on the grating, which is largely associated with the name of B. Edlen [3, 4], enabled spectroscopists to master the soft X-ray (SXR) region of the spectrum. For many decades the grating manufacturers spared no effort to maximise the equidistance of grooves, since it signified a high resolving power and was associated with the grating quality.

In 1893, M. Cornu [5] concluded that a uniform variation of the spacing of a reflection grating over its aperture changes the distance from the grating centre to different portions of the spectral focal curve*. He found that a plane grating with a

*Every imaging spectral instrument possesses two focal surfaces, i.e. spatial and spectral. By a portion of the focal surface near the instrument's principal diffraction plane is meant the locus of points characterised by the best focusing of the source image in the spatial or spectral direction. The curves formed by the intersection of spectral and spatial focusing surfaces with the principal diffraction plane will be termed the spectral (horizontal) and spatial (vertical) focal curves, respectively.

systematically varying spacing will focus the diffracted beam in the incidence of a collimated beam. In 1970, F.M. Gerasimov et al. [6] reported the fabrication of a diffraction grating with a varied spacing and its application for astigmatism compensation in a normal-incidence spectrograph. The varied groove spacing made it possible to change the position of the spectral focal curve (which now does not coincide with the Rowland circle) and to achieve its intersection with the symmetry axis of the grating (the tangent to the Rowland circle at the sphere centre – the spatial focal curve) at two points. Placed at one of these points was the entrance slit of the spectrograph, and the spectrum was observed in the vicinity of the other. This instrumental scheme provided stigmatism in the neighbourhood of only one wavelength in the visible region of the spectrum.

In the 1970s–1980s, the idea of harnessing the focusing properties of aperiodic gratings was addressed by T. Harada and T. Kita [7], M. Hettrick and S. Bowyer [8], and M. Hettrick and J. Underwood [9]. At present, the gratings with spacing monotonically varying across the aperture according to a predetermined law are called varied line-space (VLS) gratings, both plane and concave VLS gratings being used. Nowadays they enjoy wide use in optics and spectroscopy of the far VUV and SXR spectral regions. They are employed for the diagnostics of laboratory plasmas, including relativistic laser plasma, in astrophysics, microscopy and reflectometry with the use of synchrotron radiation, etc. An important feature of VLS grating spectrometers is that the spectrum is formed on a flat surface, which is almost perpendicular to the diffracted beams. This makes them compatible with modern solid-state detectors with electrical readout of the image (in particular, with backside-illuminated CCDs) and flat sensitive surfaces. Some schemes with VLS gratings are capable of constructing stigmatic spectral images in the SXR spectral region.

Several types of VLS spectrometers became commercially available (Harada spectrograph, the family of Hettrick spectrometers). However, also designed for the solution of new problems are tailor-made VLS spectrometer schemes, which take into account the specificity of scientific problems and radiation sources. This calls for a complete instrument development cycle: the calculation and optimisation of a closed optical 'source–spectrometer–detector' scheme, including calculation of VLS grating parameters and, where necessary, parameters of auxiliary mirrors, fabrication of the VLS grating and the VLS spectrometer as a whole. Such research and development is undertaken at the Lawrence Livermore National Laboratory, Lawrence Berkeley National Laboratory, Kansai Photon Science Institute, Lebedev Physical Institute (LPI), etc.

In this review we endeavour to show new possibilities that are furnished by plane and concave VLS gratings in comparison with classical gratings with equidistant grooves, to provide examples of the application of VLS gratings in modern experiments and metrology of the SXR region, and to outline the onset of work in this area at the LPI.

2. Equations describing the focusing properties of VLS gratings

The focusing properties and aberrations of a VLS grating (plane and concave) may be found using the Fermat principle, which invites calculations of the optical path function F. A plane grating may be treated as a special case of a spherical grating for $R \to \infty$. We restrict ourselves to the discussion of concave spherical and plane VLS gratings with straight grooves. For simplicity we ignore the shape of VLS grating grooves and assume them to be lines of zero width. The real groove shape is significant in the determination of intensity distribution in the spectrum.

Let the origin of the Cartesian system of coordinates coincide with the centre of a concave VLS grating (Fig. 1). Point $C(R, 0, 0)$ is the centre of the sphere on which the grating surface lies, the x axis is aligned with the normal to the grating, and the y axis is perpendicular to the grooves. The xy plane is termed the principal plane. Points $A(x, y, z)$, $B(x', y', z')$ and $P(u, w, l)$ denote a point source (for instance, an illuminated point of the entrance slit), its spectral image (at a wavelength λ), and some point of the groove on the grating surface, respectively. The grating grooves are formed in the intersection of the sphere with the planes perpendicular to the y axis. When we are dealing with a classical DG, its grooves are equidistant (along the y axis) Since point P lies on an arbitrary groove of the grating, coordinate w assumes only such values that the ratio w/d is an integer [$d = p^{-1}$ is the grating constant (period) and p is the constant groove density]. In the case of a VLS grating, the groove density is conveniently represented in the form of a polynomial

$$p(w) = p_0 + p_1 w + p_2 w^2 + p_3 w^3 + \dots , \qquad (1)$$

with $p(w) = \mathrm{d}n/\mathrm{d}w$, where $n(w) = \int_0^w p(w')\,\mathrm{d}w'$ is the groove number.

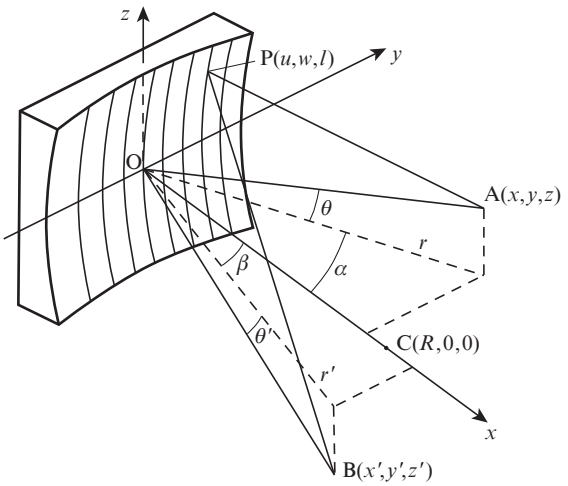

Figure 1. Concave diffraction grating: points A and B are the point radiation source and its spectral image produced by the grating; $C(R, 0, 0)$ is the sphere centre, O is the grating centre; r and r' are the projections of segments AO and BO on the principal plane xy; α is the angle of incidence and β is the angle of diffraction. The grooves of a classical grating are equidistant.

Point B is the image of point A at a wavelength λ. According to Fermat's principle, point B is so located that function F is extremal relative to small displacements of P, namely $\partial F/\partial w = 0$ and $\partial F/\partial l = 0$. If these conditions could be simultaneously satisfied for any pair of w and l, then B would be the point of perfect focus. However, a concave grating does not produce an ideal image. The point of intersection of the beam diffracting at point $P(u, w, l)$ with the focal surface, generally speaking, depends on the coordinates

of point P and deviates somewhat from the point of intersection of the central ray with this surface (from point B).

In the ideal case, the path difference between the two rays reflected from adjacent grooves is equal to an integer of the wavelength. Constructive interference of the rays (perfect focus) reflected from the grooves which are a distance w apart takes place when the path difference for these rays is precisely equal to $m\lambda n(w)$, where integer $m = 0, \pm1, \pm2, \ldots$ is called the spectral order (or the diffraction order). In this case, the expression of the optical path function APB should be of the form

$$F = l_{\mathrm{AP}} + l_{\mathrm{PB}} + m\lambda n(w). \tag{2}$$

Let us assume that the source is located close to the principal plane and take advantage of the expansion for the sum of the lengths of segments AP and PB from Ref. [10]. Then, we apply the Fermat principle to obtain

$$\frac{\partial F}{\partial w} = \left[m\lambda p(w) - \left(1 + \frac{z^2}{r^2}\right)^{-1/2} \sin\alpha - \left(1 + \frac{z'^2}{r'^2}\right)^{-1/2} \sin\beta\right] + w\left(\frac{\cos^2\alpha}{r} - \frac{\cos\alpha}{R} + \frac{\cos^2\beta}{r'} - \frac{\cos\beta}{R}\right) + \ldots = 0, \tag{3}$$

$$\frac{\partial F}{\partial l} = -\left[\frac{z}{r}\left(1 + \frac{z^2}{r^2}\right)^{-1/2} + \frac{z'}{r'}\left(1 + \frac{z'^2}{r'^2}\right)^{-1/2}\right] + l\left(\frac{1}{r} - \frac{\cos\alpha}{R} + \frac{1}{r'} - \frac{\cos\beta}{R}\right) - \frac{l}{2}\left[\frac{z^2}{r^2}\left(\frac{3}{r} - \frac{\cos\alpha}{R}\right) + \frac{z'^2}{r'^2}\left(\frac{3}{r'} - \frac{\cos\beta}{R}\right)\right] \ldots = 0, \tag{4}$$

where $p(w)$ is given by expression (1). In Eqn (3) we discarded the expansion terms containing nonzero powers of l and powers of w greater than the first, and in Eqn (4) the expansion terms containing nonzero powers of w and powers of l greater that the first. By sequentially equating to zero the different terms of expansions (3) and (4), it is possible to obtain the equations for the diffraction of the central ray (i.e. the ray passing through point O) and determine the locations of paraxial foci.

The equations that define the direction of diffraction of the central ray coincide with those for the diffraction by a classical DG, since they are obtained in the limit $w \to 0$, $l \to 0$ (we take into account that $(1 + z^2/r^2)^{-1/2} = \cos\theta$):

$$\cos\theta(\sin\alpha + \sin\beta_0) = m\lambda p_0, \tag{5}$$

$$\theta = -\theta'. \tag{6}$$

Equation (5) is often termed the grating equation. Equation (5) also signifies that the direction of diffraction of every ray is defined by the local groove density.

Equating to zero the coefficient by w in Eqn (3) gives

$$\frac{\cos^2\alpha}{r} - \frac{\cos\alpha}{R} + \frac{\cos^2\beta}{r'_{\mathrm{h}}} - \frac{\cos\beta}{R} + m\lambda p_1 = 0. \tag{7}$$

This equation describes the location of the horizontal (spectral) focus r'_{h}, which differs from the classical grating equation by the appearance of the term $m\lambda p_1$. The vertical focus location r'_{v}, as before, is described by the equation

$$\frac{1}{r} - \frac{\cos\alpha}{R} + \frac{1}{r'_{\mathrm{v}}} - \frac{\cos\beta}{R} = 0, \tag{8}$$

which is obtained by equating to zero the next, linear in l, term in Eqn (4). The vertical focus does not coincide with the horizontal one almost always (astigmatism of diffraction grating). The only nontrivial case when both paraxial foci of a classical spherical grating coincide is the Wadsworth grating mount [11].

Of greatest interest to us is the case when the source is in the principal plane or close to it, i.e. r'_{v} satisfies Eqn (8). Therefore, beginning with Eqn (7) we will imply diffraction in the principal plane in all formulae given here. We emphasise that numerical ray tracing is performed using rigorous computational formulae and does not imply the location of all source points in the principal plane.

For a plane VLS grating, Eqns (7) and (8) assume the following form:

$$\frac{\cos^2\alpha}{r} + \frac{\cos^2\beta}{r'_{\mathrm{h}}} + m\lambda p_1 = 0, \tag{9}$$

$$\frac{1}{r} + \frac{1}{r'_{\mathrm{v}}} = 0, \tag{10}$$

whence it follows that the first derivative of $p(w)$, which is equal to p_1, alters the location of the spectral focus and endows the focusing capability even to a plane diffraction grating in nonzero diffraction orders. Coefficients p_2 and p_3 in expansion (1) permit compensating for the aberration of meridional coma and spherical aberration, respectively. However, strict cancellation of each of these aberrations is possible only at one wavelength, which satisfies formulae (11) and (12):

$$m\lambda p_2 + \frac{3}{2}\left[\frac{\sin\alpha}{r}\left(\frac{\cos^2\alpha}{r} - \frac{\cos\alpha}{R}\right) + \frac{\sin\beta}{r'}\left(\frac{\cos^2\beta}{r'} - \frac{\cos\beta}{R}\right)\right] = 0, \tag{11}$$

$$mp_3\lambda + 2\left[\left(\frac{\sin\alpha}{r}\right)^2\left(\frac{\cos^2\alpha}{r} - \frac{\cos\alpha}{R}\right) + \left(\frac{\sin\beta}{r'}\right)^2\left(\frac{\cos^2\beta}{r'} - \frac{\cos\beta}{R}\right)\right] - \frac{1}{2r}\left(\frac{\cos^2\alpha}{r} - \frac{\cos\alpha}{R}\right)^2 - \frac{1}{2r'}\left(\frac{\cos^2\beta}{r'} - \frac{\cos\beta}{R}\right)^2 + \frac{1}{2R^2}\left(\frac{1}{r} - \frac{\cos\alpha}{R} + \frac{1}{r'} - \frac{\cos\beta}{R}\right) = 0. \tag{12}$$

In the instrument optimisation it is sometimes expedient to compensate for the aberrations with the use of p_2 and p_3 at two different wavelengths inside the operating spectral range. Formulae (11) and (12) were earlier given in our paper (Ref. [12]) for grazing incidence angles (formulae (8) and (9) in Ref. [12]). Unfortunately, a misprint was made in that case: the term with a factor $1/(2R^2)$ in formula (8) should have appeared in formula (9). In monograph [13] this mistake was corrected.

The term inside orders of reflection/diffraction will be used in reference to those whose rays deviate from the central

ray of the zero-order towards the incident ray. Outside orders lie on the other side of the zero order. In all cases considered below, in the detection of radiation of inside diffraction orders the groove density $p(w)$ increases in the direction from the source to the image. We also note that the odd terms of polynomial (1) $(p_1, p_3, ...)$ change sign under reversal of y-axis direction.

3. Concave VLS grating and its application. Flat-field grazing-incidence spectrometers. Harada spectrograph. Recording of high-order harmonics of femtosecond laser radiation. Emission spectroscopy

To improve the reflection efficiency in the wavelength range $\lambda < 300$ Å, gratings are quite often used at grazing incidence of radiation. In this case, the angles of diffraction are also 'grazing angles'. Then, expression (8) yields an imaginary vertical focus, $r'_v < 0$, unless the source is extremely remote from the grating or, all the more, is imaginary (i.e. unless the incident beam is converging). This signifies that the diffracted beams will be diverging vertically and hence the spectral images will be astigmatic.

In the Rowland scheme the diffracted radiation is incident on the focal surface at a small grazing angle (equal to the grazing diffraction angle, making the Rowland circle incompatible with modern CCD detector arrays (Fig. 2). One can see that detector placement on the Rowland circle entails a signal depression due to absorption in the dead layer of the detector and reflection from its surface in the grazing incidence (Fig. 2a), while detector placement normally to the incident rays (Fig. 2b) entails an impairment of focusing on the CCD detector.

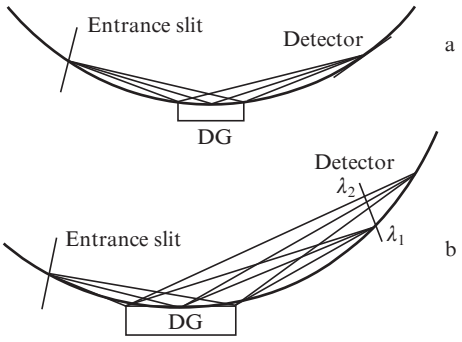

Figure 2. Versions of CCD detector usage in the grazing incidence Rowland scheme with a classical concave grating: (a) the Rowland circle is tangent to the CCD detector surface and the diffracted radiation is incident on the detector at small grazing angles, with the result that the path in the dead (absorbing) detector layer becomes longer and a significant fraction of the signal is lost in it; (b) the detector is placed normally to diffracted rays, which improves detection efficiency but entails a significant impairment of the focusing and a lowering of resolving power.

Efficient (both from the standpoint of detection and resolving power) use of a concave grating in combination with a CCD detector calls for an alteration of the spectral focal curve with an appearance of a straight segment oriented almost normally to the direction of propagation of diffracted radiation. The spectral instruments that satisfy this requirement are called flat-field spectrometers. To modify the spectral focal curve, advantage can be taken of a VLS grating. Figure 3 is a schematic of a grazing incidence flat-field spectrometer with a spherical VLS grating. Here, we go over to the use of grazing angles of incidence and diffraction, which are related to angles α and β by the obvious relations:

$$\varphi = \pi/2 - \alpha, \quad \psi = \pi/2 + \beta. \tag{13}$$

The sign + in the second formula implies that angle β is negative when the source and its image are located on different sides of the grating normal drawn at its centre (we assume that $\alpha > 0$).

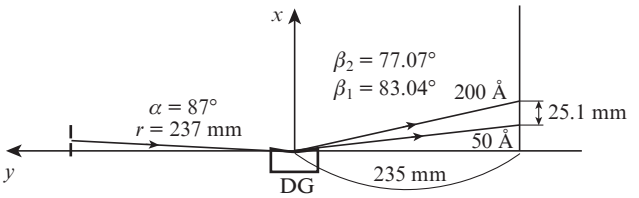

Figure 3. Schematic of a Harada spectrograph [14]. A spherical VLS grating with a radius of curvature of 5649 mm, $p_0 = 1200$ mm^{-1}, and aperture of 5 cm forms a rectilinear segment of the focal curve in the 50–200 Å wavelength range, with angles of incidence on the detector ranging between 7° and 13°.

In 1980, T. Harada [7] designed the first instrument of this kind for the wavelength range 50–200 Å. For a dispersive element he employed a spherical ($R = 6$ m) concave VLS grating with a central groove density $p_0 = 1200$ mm^{-1}. The angle of grazing incidence on the grating was equal to 3°. The spacing varied from 1.0 to 0.71 μm across the 5-cm aperture. In this case, between 50 and 200 Å the spectral focal curve was nicely approximated with a straight segment perpendicular to the y axis, and the angles of incidence of diffracted rays ranged from 7° to 13° [7]. More recently, after some modification of parameters ($R = 5649$ mm, the spacing varies between 0.99 and 0.69 μm), the instrument operation was demonstrated in the recording of laser-plasma spectra [14]. It became commercially available and has come to be known as a Harada spectrograph (see Fig. 3) and received worldwide acceptance.

To exemplify the use of the Harada spectrograph we cite the recording of high-order laser harmonics generated in relativistic helium plasma produced by the radiation of a multiterawatt femtosecond J-KAREN laser with an intensity above 10^{18} W cm^{-2} [15] (Fig. 4). A helium jet is directed perpendicular to the drawing plane. A toroidal mirror images the SXR radiation source onto the input of the Harada spectrograph (horizontal focus), while the vertical focus is on the detector. Generated in this case were both odd and even harmonics, and their frequencies were multiples of the base frequency ω_f, which was somewhat lower than the carrier frequency of a Ti:saphhire laser (Figs 5 and 6) [15]. A high quality of the recorded spectra permitted formulating the hypothesis that the harmonics were generated by density singularities produced in the multiflux plasma motion. This hypothesis was experimentally borne out in Ref. [16] by recording the images and spectra of coherent point sources in the 12–20 nm spectral range. Such sources are the special case of a more general phenomenon, which received the

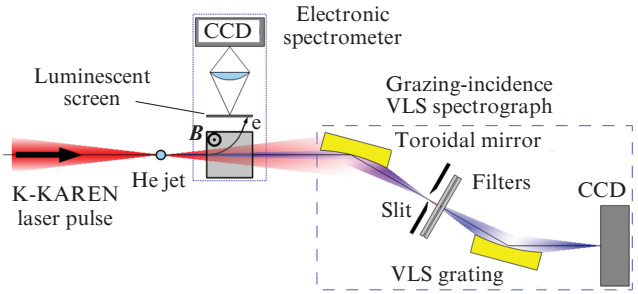

Figure 4. Schematic of a facility for recording high-order harmonics of multiterawatt femtosecond laser radiation [16]. The harmonic spectrum, which lies in the far VUV and SXR range, is recorded with a flat-field VLS spectrometer.

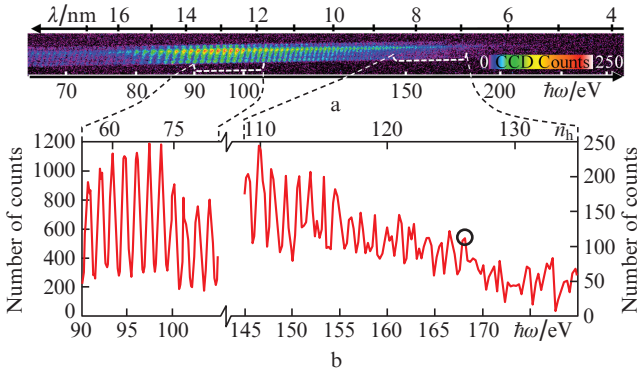

Figure 5. (a) Typical harmonic spectrum of Ti:sapphire laser radiation obtained for a laser power of $P_0 = 9$ TW and a peak electron density $n_e = 4.7\times10^{19}$ cm^{-3} in the helium plasma [16] as well as (b) results of processing of two selected portions of the spectrum. The harmonic frequencies $n_h\omega_f$ are multiples of the base frequency $\omega_f = 0.885\omega_0$, where ω_0 is the frequency of laser radiation. The greatest number of a clearly discernible harmonic n_h^* is shown with a circle.

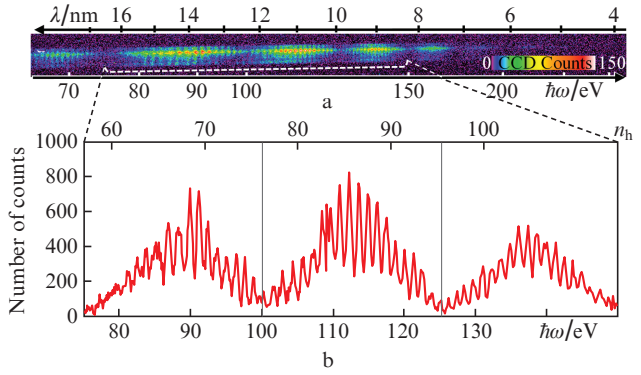

Figure 6. (a) Typical modulated harmonic spectrum for $P_0 = 9$ TW, $n_e = 4.7\times10^{19}$ cm^{-3}, $\omega_f = 0.872\omega_0$ [16] as well as (b) result of processing of selected portion of the spectrum. Vertical lines show the modulation period $\Delta\omega = 19\omega_f$.

name BISER (Burst Intensification by Singularity Emitting Radiation) [17].

At the Rutherford Appleton Laboratory (Great Britain), a slitless version of the VLS spectrometer was also employed to record the harmonics. Neely et al. [18] described a slitless three-channel flat-field VLS spectrometer for the 5–90 nm range. One of its purposes was to estimate the angular distribution of the harmonic radiation (Fig. 7). Three grazing-incidence mirrors, which were endowed the shape of elliptical cylinders, intercept the harmonic radiation emanating at angles of 0±13, 46±21, and 108±35 mrad. The mirrors are crossed relative to the grating and each constructs a one-dimensional image of the X-ray source on the detector, while the concave Hitachi grating ($R = 5649$ mm, width: $W = 50$ mm) constructs its spectral images, which are dispersed and focused in the perpendicular direction. The instrument is therefore a flat-field stigmatic (imaging) VLS spectrometer.

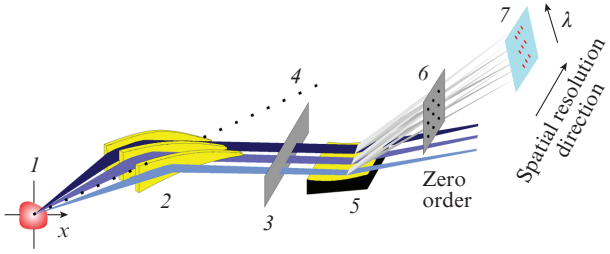

Figure 7. Three-channel flat-field slitless imaging spectrometer with a spherical VLS grating:
(*1*) X-ray source; (*2*) grazing-incidence mirrors in the form of elliptical cylinders; (*3*) prefilter; (*4*) axis; (*5*) concave aperiodic flat-field VLS grating ($p_0 = 1200$ mm^{-1}); (*6*) X-ray filter; (*7*) CCD detector (5–90 nm). (Adapted from Ref. [18].)

Beiersdorfer et al. [19] reported the development of a flat-field grazing-incidence (angle $\varphi \sim 2°$) VLS spectrometer for a range of 10–50 Å. They employed a VLS grating with a long radius of curvature ($R = 44.3$ m) and an average groove density of 2400 mm^{-1}, which varied from 2270 to 2540 mm^{-1} across the aperture. A high linear dispersion was achieved due to long 'slit–grating' and 'grating–detector' distances as well as due to a high groove density. The overall length of the instrument amounted to about three metres. The spectrometer was intended for recording SXR spectra excited in an electron beam ion trap (EBIT) at the Lawrence Livermore National Laboratory (LLNL, USA). It was noted that the spectrometer provided a higher resolving power in the specified spectral range (600 at $\lambda = 16$ Å and 1200 at $\lambda = 35$ Å) than the existing grating spectrometers and complemented short-wavelength crystal spectrographs from the standpoint of spectral range coverage and polarisation-independent response.

More recently, a similar flat-field grazing-incidence VLS spectrometer for the 10–50 Å range was implemented at the LLNL. The instrument was intended for recording spectra excited in the laser plasma of various targets [20]. A cooled CCD matrix was used as a detector. Given in Ref. [20] are excellent Lyman series spectra of the H- and He-like oxygen ions (including dielectronic satellites) excited in the laser irradiation of a 3-μm thick lavsan film and a 300-μm aerogel layer with a density of 50 mg cm^{-3}. A spectral resolving power above 1200 was reached in the $\lambda \sim 19$ Å domain.

VLS gratings are also employed in SXR emission spectroscopy (SXES) combined with an electron microscope [21–23]. In this case, the radiation is excited by a focused electron beam, which permits recording spectra with a high spatial resolution. The application of VLS gratings enables the spectral resolution and instrument sensitivities to be significantly

Table 1. Parameters of VLS gratings for SXES spectroscopy [23].

Energy range/eV	Wavelength range/nm	The angle of grazing incidence/deg	p_0/mm^{-1}	Radius of curvature/mm	Coating
50–200	25–6	4	1200	3960	Au
155–350	8.0–3.5	2.93	1200	5606	Ni
300–2200	4.13–0.56	1.35	2400	13800	Au
2000–4000	0.62–0.33	1.35	2400	11200	Mo/C multilayer, period 5.2 nm, about 30 periods [22]

improved in the detection of impurities and evaluation of chemical bonds. The combination of an electron microscope and a SXR spectrometer is widely used in materials science, in the development of new energy storage systems (for instance, lithium–ion batteries), etc. Imazono et al. [23] designed a half-metre spectrograph for SXES with four interchangeable VLS gratings, which spanned a wavelength range almost two orders of magnitude wide (Table 1). The operating spectral range begins from the K line of Li (54 eV) and encompasses, in particular, the M lines of Pt: M_α (2050 eV) and M_β (2127 eV). The resolving power of the instrument was measured in experiments with a laser-plasma source of line radiation and was equal to ~1000 near 40 eV and no less than 700 near the K line of Li. Also recorded was the K spectrum of metallic lithium excited in an electron microscope. SEM-SXES (Scanning Electron Microscope–Soft X-ray Emission Spectrometer) instruments are commercially available [24].

4. Plane VLS grating and its application. High- and ultrahigh-resolution grazing-incidence scanning spectrometers/monochromators with a plane VLS grating. Measurement of the laser linewidth of Se XXV ions (206.38 Å). Hettrick spectrometers. Monochromatisation of synchrotron radiation

Another class of VUV and SXR instruments in demand are monochromators and spectrometers with a high spectral resolution, a constant deviation angle, and immobile entrance and exit slits (or detector in place of the exit slit), in which the frequency is scanned by rotation of a plane VLS grating. The idea of this approach was conceived by Hettrick and Underwood [9].

Experimentally, the use of instruments with invariable directions of entrance and exit of radiation (i.e., with a constant deviation angle Ω) and invariable distances to the input and output slits (or to the radiation detector) is superior to the use of instruments in which wavelength scanning calls for significant changes of the facility configuration. In a scheme with a constant deviation angle, the angle of incidence of the central ray on the grating is related to the wavelength by the expression

$$\sin\alpha - \sin(\alpha + \Omega) = mp_0\lambda,$$

or

$$\alpha = \arccos\left(\frac{-mp_0\lambda}{2\sin(\Omega/2)}\right) - \frac{\Omega}{2}. \qquad (14)$$

As is well known, the advantage of using an outside diffraction order in a scheme with a constant deviation angle is that the passage to shorter wavelengths is performed by decreasing the grazing angle $\varphi = \pi/2 - \alpha$ of incidence on the grating, making it possible to maintain the reflection coefficient at a sufficiently high level. Next we consider the position of the output slit (of the spectral focus). Let the line density vary by the law $p = p_0 + p_1 w$ (higher-order expansion terms in w do not affect the focusing in the paraxial approximation) and let a converging radiation beam of wavelength λ be incident on a plane VLS grating at an angle α. If the distance of the incident beam focus from the grating centre is r, on reflection the beam focuses at a distance r'_h defined by Eqn (9), where r now is conveniently assumed to be positive and the y axis in Fig. 1 directed in the opposite direction:

$$-\frac{\cos^2\alpha}{r} + \frac{\cos^2\beta}{r'_h} = m\lambda p_1, \text{ or } r'_h = r\frac{\cos^2\beta}{\cos^2\alpha + mp_1\lambda r}. \qquad (15)$$

The constancy condition for the distance r'_h may be fulfilled for two wavelengths (λ_1, λ_2) for an invariable distance to the focus of the initial beam in the scheme with a constant deviation angle. Coefficient p_1 characterises the grating and is invariable. Then

$$p_1 = \left[-\frac{\cos^2\alpha_1}{r} + \frac{\cos^2\beta_1}{r'_h}\right]\frac{1}{m\lambda_1}$$

$$= \left[-\frac{\cos^2\alpha_2}{r} + \frac{\cos^2\beta_2}{r'_h}\right]\frac{1}{m\lambda_2}, \qquad (16)$$

whence we obtain

$$\frac{r'_h}{r} = \frac{\lambda_2\cos^2\beta_1 - \lambda_1\cos^2\beta_2}{\lambda_2\cos^2\alpha_1 - \lambda_1\cos^2\alpha_2}. \qquad (17)$$

Considering that $m\lambda_{1,2} = (\sin\alpha_{1,2} + \sin\beta_{1,2})/p_0$, we obtain the relation

$$\frac{r'_h}{r} = \frac{(\sin\alpha_2 + \sin\beta_2)\cos^2\beta_1 - (\sin\alpha_1 + \sin\beta_1)\cos^2\beta_2}{(\sin\alpha_2 + \sin\beta_2)\cos^2\alpha_1 - (\sin\alpha_1 + \sin\beta_1)\cos^2\alpha_2}. \qquad (18)$$

Relations (16)–(18) were obtained by eliminating parameter p_1, which is no longer a free parameter. One can see from expressions (18) and (14) that it is possible to select the deviation angle Ω and angles of incidence $\alpha_{1,2}$ (or, which is the same, wavelengths $\lambda_{1,2}$) for a fixed p_0. On fixing the above parameters it is possible to arbitrarily select the overall length of the instrument [considering that r'_h/r is already defined by relation (18)] and thereby define coefficient p_1 by relation (16).

The simplest scheme of a scanning VLS spectrometer/monochromator comprises an entrance slit, a concave spherical mirror for radiation focusing in the grating dispersion plane, a VLS grating, and an exit slit (or a detector in spectrometer mode). The VLS grating is most often (but not necessarily) used in the first outside order.

Given below is our calculated scheme of a metre scanning spectrometer/monochromator with a working spectral range 100–300 Å, which possesses the limiting theoretical ($\lambda/\delta\lambda = pW = 30000$) resolving power throughout the entire working range (Fig. 8). The entrance slit is placed on the Rowland circle of the mirror. The concave grazing-incidence mirror forms the horizontal focus of the slit image behind the VLS grating. The angle of grazing incidence and the radius of curvature of the mirror are selected from considerations of desired reflectivity and requisite instrument size. The grating is placed in the converging beam. The positions of the entrance slit and exit slit (or detector) is invariable in the scanning, which is performed simply by VLS grating rotation. The law which describes the groove density variation, as before, is of the form $p(w) = p_0 + p_1 w + p_2 w^2 + p_3 w^3$.

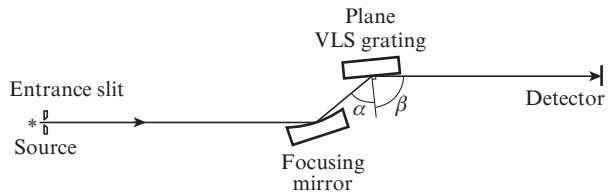

Figure 8. Scanning VLS grating spectrometer/monochromator with a constant deviation angle.

As is well known, a monochromator with a constant deviation angle and immobile slits can be made with the use of a classical spherical grating. Let us assume that use is made of the Rowland scheme, the position of the exit slit corresponding to some λ_0. Then, the geometrical defocusing rapidly increases in the rotation of the grating and the resolution declines. If the exit slit is placed outside of the Rowland circle, paraxial rays now are focused at two wavelengths $\lambda_{1,2}$, but even at these wavelengths the resolution is limited by meridional coma and spherical aberration in this case. Figure 9 shows the width (in μm) of the spectral images produced by the scanning VLS spectrometer/monochromator and the monochromator with a classical spherical DG, which were obtained by numerical ray tracing. In the VLS grating monochromator the width of the geometrical image is narrower than the diffraction-limited width throughout the working range, which is broader than an octave in wavelength. That is why the spectral resolving power coincides with the theoretical limit defined by the number of DG grooves: $\lambda/\delta\lambda = pW = 30000$.

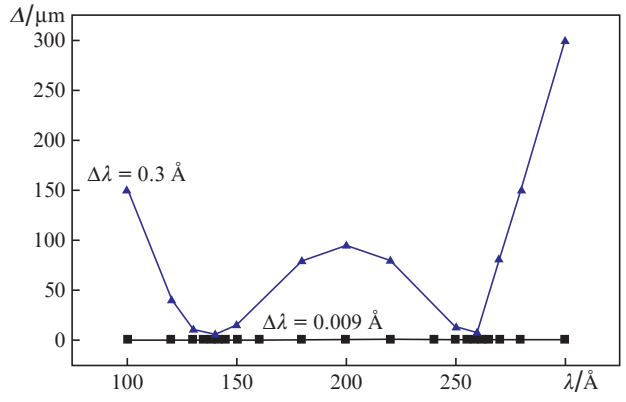

Figure 9. Width of the spectral image of a point source calculated by numerical ray tracing for monochromators with a classical concave DG with $p = 600$ mm^{-1} (▲) and a VLS grating with $p_0 = 600$ mm^{-1} (■). In both cases, the grating width is assumed to be equal to 5 cm and the 'grating–detector' distance to be 1 m; $\Delta\lambda$ is the spectral resolution.

The first scanning spectrometer with a plane VLS grating with $p_0 = 1800$ mm^{-1} was reported in Ref. [25], where a super-high resolving power was demonstrated in a broad wavelength range: ~16000 near ~130 Å, ~35000 near ~160 Å, and ~30000 near 208 Å. Used in the measurements were narrow lines of Al IV (130 and 160 Å) and Ne IV (208 Å) ions excited in a glow discharge in a longitudinal magnetic field (Penning discharge). Subsequently the scanning spectrometer was repeatedly employed in experiments. One of the most impressive applications of the instruments of this type is the measurement of the radiation linewidth of the X-ray laser operating by the transition of Ne-like Se ion (206.38 Å) [26]. It was possible to demonstrate the $\lambda = 206.38$ Å line narrowing from 50±10 mÅ to about 10 mÅ with increasing the length l of the amplifying medium (the length of the plasma of multiply charged Se ions) from 0.5 to 6 cm.

The scanning spectrometer/monochromator possesses several remarkable properties. The wavelength scanning is achieved simply by grating rotation with retention of a high spectral resolving power (10^4 and over) throughout a broad wavelength range (more than an octave). In doing this, the remaining elements of the instrument remain immobile. The portion of the focal surface corresponding to the direction of recording remains practically immobile and perpendicular to the diffracted rays. The latter circumstance makes these instruments ideally compatible with modern radiation detectors, CCD detectors in particular. Due to the indicated combination of properties the scanning spectrometers/monochromators with a plane VLS grating have received wide acceptance and become commercially available [27].

Nowadays plane VLS gratings are used in monochromators with a constant deviation angle and immobile slits in the operation with synchrotron radiation. One of such schemes is depicted in Fig. 10, where the monochromator is a part of a reflectometer [28]. To cover as broad as possible a wavelength range (9.5–250 Å, or 50–1300 eV), use was made of three interchangeable VLS gratings with average line densities $p_0 =$ 300, 600, and 1200 mm^{-1}.

In the measurement of VLS grating efficiencies in Ref. [28] it turned out, in particular, that the gratings made by interference lithography exhibited a lower radiation scattering than the gratings made with a mechanical ruling engine.

To investigate the electronic structure of a condensed substance by angle-resolved photoelectron spectroscopy (ARPES), a radiation channel was designed on the Shanghai synchrotron, which comprises a VLS monochromator for an energy range of 7–791 eV [29]. The VLS monochromator makes use of three plane VLS gratings with $p_0 = 190$ mm^{-1} (DG1, 7–104 eV), 620 mm^{-1} (DG2, 17–244 eV), and 2000 mm^{-1} (DG3, 55–791 eV). The scheme of this monochromator is different from that used in Ref. [28]: the mirror in front of the grating is flat, the focusing in the plane of dispersion is imposed entirely on the VLS grating, and wavelength scanning is effected by combined rotation of the mirror and the grating. For each grating, the calculated resolving power depends on the wavelength but remains sufficiently high. For the DG1–DG3 gratings, in the specified energy ranges it varies in the limits $(8.3–7.3)\times10^3$,

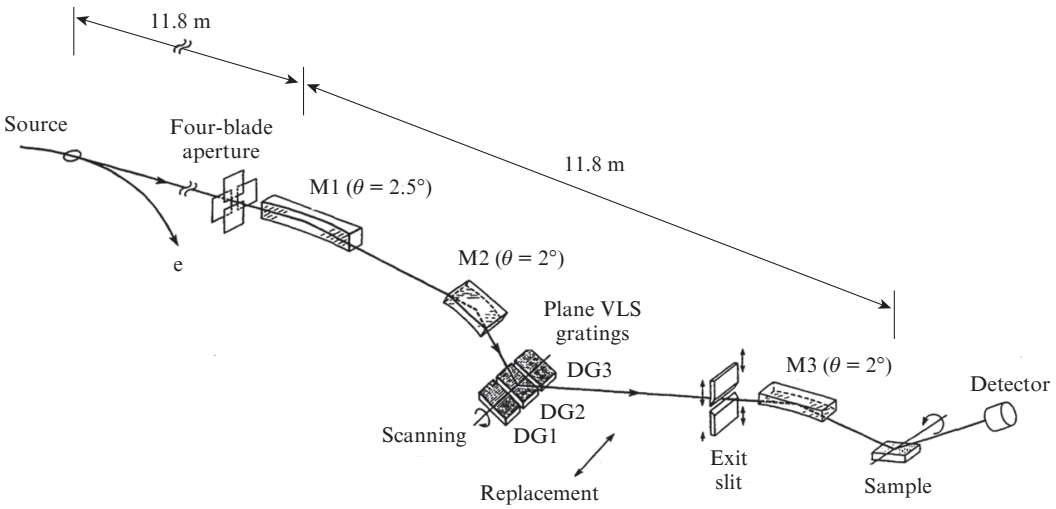

Figure 10. Schematic of a reflectometer based on a monochromator with interchangeable plane VLS gratings (DG1 – DG3), which uses synchrotron radiation: (M1, M2) grazing-incidence spherical mirrors; (M3) cylindrical grazing-incidence spherical mirror; $\Omega = 8°$ (Adapted from Ref. [28].)

$(2.4-1.8)\times10^4$, and $(3.8-2.0)\times10^4$, respectively. To improve the efficiency, it is planned to employ gratings, whose profile density varies along the groove.

Ranking with the above facility is the project of a synchrotron radiation channel (National Synchrotron Radiation Laboratory, Suzhou, PRC) intended primarily for the investigation of nanomaterials and their application in energy conversion/storage and catalysis studies by X-ray absorption spectroscopy and optical luminescence under X-ray irradiation [30]. The designed energy range (100 – 1000 eV) contains the K edges of light elements (C, N, O, F) and the L edges of transition metals (Fe, Co, Ni). It is planned to employ two plane VLS gratings with p_0 = 840 and 1400 mm^{-1} in the ranges 60 – 600 and 100 – 1000 eV, respectively. The calculated resolving power of the monochromator in these ranges varies from ~3000 to ~1300 for both gratings. Like in Ref. [29], the plane VLS grating is the only focusing element of the monochromator, but scanning is performed by rotation of only one plane mirror placed in front of the grating.

Along with synchrotron radiation, use is also made of a laser-plasma radiation source. For instance, a laboratory reflectometer was made for the characterisation of components of projection X-ray microlithography systems [31]. This reflectometer with a constant deviation angle $\Omega = 20°$ employs a gold-coated VLS grating with p_0 = 2400 mm^{-1} made by interference lithography.

5. Stigmatic (imaging) spectrometers with a grazing-incidence plane VLS grating. Application in X-ray/VUV astrophysics. Broadband spectrometer with strict astigmatism compensation at two wavelengths

We consider a plane classical reflection grating placed in a converging homocentric beam. As is commonly known, a DG with equidistant grooves introduces significant astigmatism in this scheme (Fig. 11), i.e. the spatial positions of the spectral (horizontal) and vertical foci do not coincide. The vertical focus lies on a circle described about point O, its radius L being equal to the length of segment OF, i.e. the distance of the beam focus from the grating centre. For inside diffraction orders ($m > 0, \psi > \varphi$), the spectral focus A lies outside of this circle (OA > OF), and for outside order ($m < 0, \psi < \varphi$) it lies inside the circle. The distance of the mth-order spectral focus from the grating centre is defined by the formula

$$L_m = L\frac{\sin^2\psi_m}{\sin^2\varphi}, \tag{19}$$

and the smaller the grazing-incidence angle, the stronger the astigmatism. Relation (19) follows from formula (9) for $r'_h < 0$ (an imaginary source) and $p_1 = 0$ on going over to grazing angles of incidence and diffraction.

It is well known that the use of a VLS grating in a converging beam permits eliminating astigmatism at one wavelength λ_0. For a plane VLS grating irradiated by a converging homocentric beam, Hettrick and Bowyer [8] defined the law

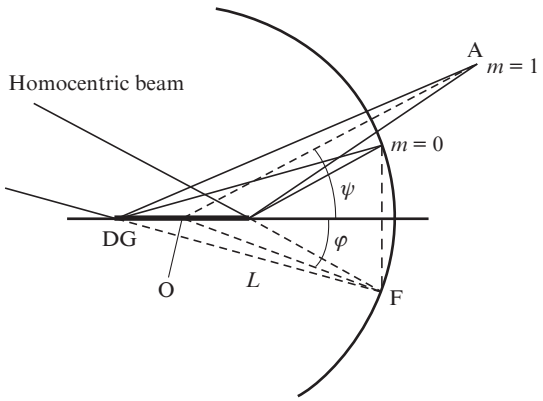

Figure 11. Astigmatism of a grazing incidence plane DG with equidistant grooves: L – distance of the focus F of converging homocentric beam from the grating centre (point O); the vertical focus of diffracted beams lies on the circumference of radius L described about the grating centre O; A is the spectral focus for the first inside order.

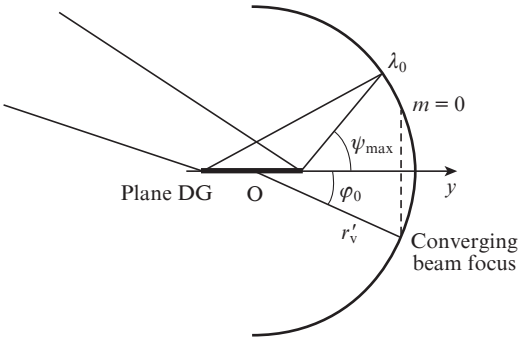

Figure 12. Fulfilment of the stigmatic condition at a wavelength λ_0 due to groove spacing variation across the aperture of a plane VLS grating, which is placed in a converging homocentric beam, according to Eqn (15).Like with a classical DG, the vertical focus of diffracted beams lies on the circumference of radius r'_v described about the grating centre O; inside diffraction order; the groove spacing decreases in the direction of y axis.

of spacing variation which brings into coincidence the spectral and vertical foci at a preselected wavelength (Fig. 12):

$$\frac{1}{p(w)} = d(w) = \frac{m\lambda_0}{\cos\varphi(w) - \cos\psi(w)}, \qquad (20)$$

where $\varphi(w)$ and $\psi(w)$ are local grazing incidence angles of incidence and diffraction. The rays that lie in the principal plane diffract in the requisite direction from any point with coordinate w in the y-axis to produce the point image of a point source at a wavelength λ_0. In this case, the distance between the spectral (horizontal) and vertical foci increases as the wavelength recedes from λ_0 (Fig. 13).

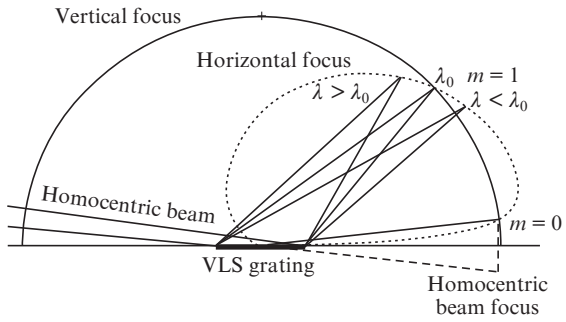

Figure 13. Curves (loci) of horizontal and vertical foci in the incidence of a converging homocentric beam on a plane VLS grating. The divergence of the foci increases as the wavelength recedes from λ_0.

For the first time, plane VLS gratings were presumably applied in astronomy in the 1990s. The scheme of a spectrometer with three plane VLS gratings, in which a converging homocentric beam was formed by an X-ray telescope, was employed to obtain the map of extrasolar radiation sources in the far VUV spectral domain ($\lambda \sim 100$–1000 Å) on board the artificial Earth satellite EUVE (Extreme Ultraviolet Explorer, NASA Observatory) [32–35].

The principal objective of the project was to find and identify extrasolar sources in the far VUV spectral domain. The homocentric beam that gave rise to the image of a remote source was produced by a grazing-incidence Wolter–Schwarzschild type-2 telescope with a focal length of 136 cm [32]. Half of its annular aperture served to illuminate a deep-survey detector, while the other half was intercepted by three VLS gratings (1/6 of the aperture each) designed for three spectral subranges, each about an octave in width. Therefore, the spectral images of extrasolar sources were constructed in three channels (A, B, C). In the spectral channels A (70–190 Å), B (140–380 Å), and C (280–760 Å), use was made of VLS gratings with ruled areas measuring 80×200 mm and groove densities of 1675–3550, 830–1750, and 415–875 mm^{-1}, respectively. Detectors were placed in the focal plane of the telescope. To suppress the undesirable background caused by the scattering of hydrogen Ly$_\alpha$ line (1216 Å) and the UV stellar radiation, a thin-film filter was placed in front of each detector. Furthermore, placed in front of the telescope were collimators, which limited the field of view and prevented from spectrum contamination by the diffuse radiation of the resonance lines of He I (584 Å) and He II (304 Å).

On 7 July 1992, the EUVE observatory was successfully put into orbit of height 550 km with an inclination of 28° relative to the equatorial plane of the Earth to become the first observatory for the observation of extrasolar objects in the far VUV and SXR spectral domains. As a result of nine-year observatory operation, a large number of radiation sources were detected (734 in all), their far VUV and SXR spectra were recorded, and catalogues of the sources and their spectral lines were published. The literature on this subject is quite extensive (see, for instance, Refs [33–35] and references therein). The general picture, which graphically depicts the distribution of extrasolar far-VUV and SXR radiation sources, is given in Ref. [36].

It is possible to design a quasi-stigmatic spectrometer by sending a slightly astigmatic beam to a plane VLS grating rather than a homocentric one, like in Figs 12 and 13. The conception of this instrument was elaborated in Ref. [37], with a rigorous astigmatism compensation being achieved at two wavelengths and a practical stigmatic condition in a broad spectral range of about two octaves. We implemented a spectrometer of this kind in the $\lambda > 12$ range with the use of a plane VLS grating ($p_0 = 600$ mm^{-1}) and a concave ($R = 1$ m) multilayer mirror (MM) [38–40] (Fig. 14). The function of producing a slightly astigmatic beam is imposed on a broad-

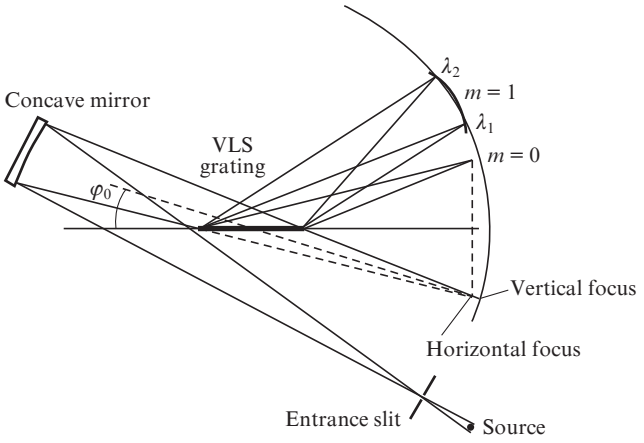

Figure 14. Optical scheme of a broadband imaging spectrometer comprising a concave focusing aperiodic MM and a plane VLS grating.

band normal-incidence mirror based on an aperiodic Mo/Si multilayer structure optimised for maximum uniform reflectivity in the 125–250 Å range [41]. Given below are the parameters of the stigmatic spectrometer for the 12.5–30 nm range.

Angle of central ray incidence on the MM/deg	7.59
Radius of MM curvature/mm	1000
MM diameter/mm	50
Spectral MM reflectivity range/Å	125–300
Grazing angle φ/deg	6.44
Wavelength λ_1 of strict stigmatism/Å	144
Grazing angle of diffraction at a wavelength λ_1/deg	9.92
Wavelength λ_2 of strict stigmatism/Å	272
Grazing angle of diffraction at a wavelength λ_2/deg	12.21
Plasma–entrance slit distance/mm	30
Entrance slit–MM distance/mm	991.2
MM–VLS-grating distance/mm	461.2
Distance L_h of the horizontal MM focus from the VLS grating/mm	530.0
Distance L_v of the vertical MM focus from the VLS grating/mm	535.5
p_0/mm^{-1}	600
p_1/mm^{-2}	2.2
p_2/10^{-3} mm^{-3}	6.0
Plate scale at a wavelength λ_1/Å mm^{-1}	5.36
Resolving power at wavelength λ_1 defined by one detector pixel	2070
Plate scale at a wavelength λ_2/Å mm^{-1}	6.5
Resolving power at wavelength λ_2 defined by one detector pixel	3200
Size of illuminated grating surface/mm	
width	40
height	18
Acceptance angle/sr	2.9×10^{-4}
Vertical field of view/mm	no less than 10

In the implemented scheme, both the horizontal (spectral) focus of the entrance slit and the vertical (spatial) image of laser plasma are on the surface of the detector, the plasma being located 30 mm in front of the entrance slit. Recorded in experiment is therefore the spectrum resolved spatially in the vertical direction (along the slit).

The spectra were recorded with backside-illuminated CCD detectors (number of 13-μm sized pixels: 2048×1024; number of 13.5-μm sized pixels: 2048×512). In the first experiments, use was made of a VLS grating made by electron beam lithography at the Centre for Shared Use of the MIPT. Line spectra of the multiply charged ions Li III and F V–F VII were recorded in laser-produced plasma and spectral resolving power $\lambda/\delta\lambda \approx 500$ was demonstrated. In this case, the spatial resolution was equal to ~26 μm, or two detector pixels. Subsequently, use was made of a VLS grating made by interference lithography at the Institute of Applied Optics (Kazan). Resolving power $\lambda/\delta\lambda \approx 10^3$ was obtained with the use of this grating [39, 40], which also corresponds to two detector pixels and is therefore the limit for a one-metre spectrograph equipped with a $p_0 = 600$ mm^{-1} grating. By way of example Fig. 15 shows the line spectrum of multiply charged ions of fluorine and lithium obtained in the irradiation of a LiF target in one laser shot. Owing to stigmatism and a relatively large acceptance angle of 2.9×10^{-4} (see above), the instrument exhibits a high luminosity. For a more detailed description of the experiment and instrument design the reader is referred to Ref. [39].

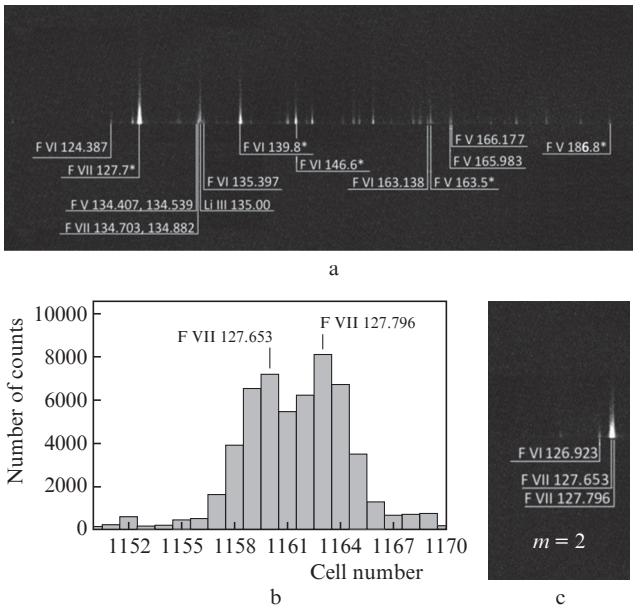

Figure 15. (a) Plasma spectrum with spatial resolution in the normal direction to the target recorded by focusing a laser pulse (0.5 J, 8 ns, 1.06 μm) on a LiF target (the VLS grating was made by interference lithography), (b) histogram of F VII lines in the second diffraction order, and (c) resolvable lines of F VI and F VII ions in the second diffraction order. The spectral resolving power $\lambda/\delta\lambda \approx 10^3$, the spectral and spatial resolutions both corresponding to two detector pixels (26 μm).

Note in conclusion of this Section that the further improvement of the instrument parameters is possible by advancing the VLS-grating production technology. In this case, the limiting practical spectral resolving power will be defined by the product of the detector pixel size and the plate scale, which may range up to 2000 and more, depending on the specific scheme parameters. The limiting spatial resolution of the scheme in Fig. 14 is also limited by the detector pixel size. A higher spatial resolution could be attained by imaging the source on the detector with a magnification, which is a non-trivial task in the XUV range.

6. Other applications of plane VLS gratings. X-ray fluorescence analysis, microscopy, resonant inelastic X-ray scattering spectroscopy

A start has been made on the application of flat-VLS-grating spectrometers to the study of molecules, materials, and biological objects by resonant inelastic X-ray scattering (RIXS).

A broadband flat-field SXR spectrometer with a plane VLS grating was made for the spectral range 130–650 eV (19–95 Å) [42]. The spectrometer is intended for the investigation of radiation-sensitive biological samples placed in a focused synchrotron radiation beam. The slitless spectrometer is made according to the Hettrick–Underwood scheme and comprises a spherical mirror and a plane VLS grating operating (unlike the scanning Hettrick–Underwood spectrometer/monochromator [9]) in the inside diffraction order (Fig. 16). The second significant difference is that the mirror directs a diverging beam to the grating rather than the converging one. The instrument records the radiation simultaneously (i.e., without any mechanical motion) throughout the working spectral range with a resolving power of no less than 1200

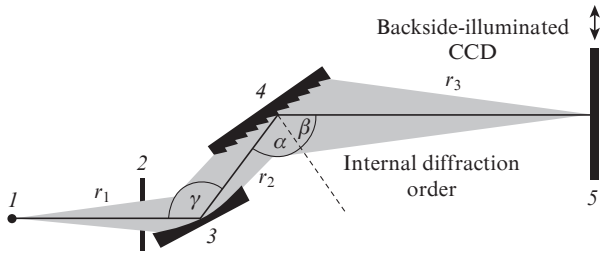

Figure 16. Schematic of a plane-VLS-grating SXR spectrometer for the 19–95 Å range:
(*1*) radiation source (the focus of a synchrotron radiation beam on a thin sample under investigation); (*2*) aperture stop; (*3*) spherical mirror mounted at a grazing incidence angle of 4° ($\gamma = 172°$); plane VLS grating ($p_0 = 600$ mm^{-1}) with a blaze angle of 1.8° placed at a grazing angle of 2.1° ($\alpha = 87.9°$) and operating for a grazing diffraction angle of 5.9° ($\alpha + \beta = \gamma = 172°$). The sensitive detector surface *5* is perpendicular to the axis of the incident beam. (Adapted from Ref. [42].)

realised provided the that the radiation source does not exceed 30 μm × 3 mm. The high efficiency of the instrument permits recording two-dimensional RIXS maps in several minutes.

The spectrometer described above [42] is optimised to the absorption edges of the elements which primarily make up organic materials. The instrument is designed to record the radiation in the vicinity of the L edge of sulphur ($L_{2,3}$, 150 eV) in the first diffraction order, in the vicinity of the K edge of carbon (280 eV) in the second order, and in the vicinity of the K edges of nitrogen (400 eV) and oxygen (525 eV) in the third diffraction order. Owing to the use of three diffraction orders at different wavelengths, the indicated spectral regions are rather closely located on the detector.

Another example of the application of a high-resolution plane-VLS-grating spectrometer to the recording of resonant inealastic X-ray scattering is provided by Ref. [43]. It is dedicated to the development of a sophisticated imaging VLS spectrometer with a resolving power of 30000 in the 680–740 eV range. The overall VLS spectrometer length is about 5 m. The radiation emanating from an object is collected and directed to the plane VLS grating with the use of a system of three grazing-incidence mirrors. The first two mirrors (a hyperbolic cylinder and an elliptic cylinder) produce on the detector the vertical focus of the source, while the third mirror (an elliptic cylinder) focuses the radiation of the source in the horizontal direction (in the dispersion plane) and directs the converging beam to the grating (Fig. 17). The total magnification of the scheme is equal to about 10 in the dispersion plane (horizontally) and about 5 in the crossed direction (vertically). The VLS grating is placed at a grazing angle of 8° and operates in the outside order $m = -1$ for a grazing diffraction angle of 2.4°.

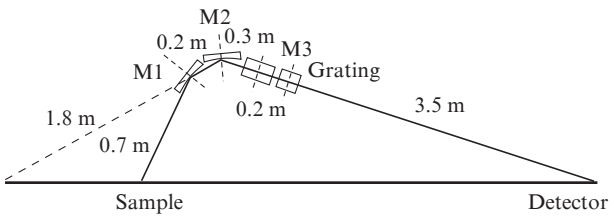

Figure 17. Vertical section of the plane-VLS-grating SXR spectrometer for the range 680–740 eV with a spectral resolving power of 30000: M1 and M2 (a hyperbolic cylinder of width 150 mm and an elliptic cylinder of width 150 mm) provide vertical focusing, M3 (an elliptic cylinder of width 320 mm) furnishes horizontal focusing (in combination with the VLS grating of width 75 mm). (Adapted from Ref. [43].)

7. VLS-grating fabrication technologies

The first fabrication of high-quality diffraction gratings with a spacing monotonically varying over the aperture was presumably reported by F.M. Gerasimov et al. [6], who described the fabrication of mechanically ruled gratings (R =1 m, p_0 = 600 mm^{-1}) with a total relative variation of the spacing of the order of $\sim 10^{-2}$. This relatively small variation of the spacing may provide astigmatism compensation in normal-incidence schemes.

In 1975–1976 T. Harada et al. (Central Research Laboratory, Hitachi Ltd., Tokyo) [44, 45] reported the development of a programmable ruling engine capable of varying the groove spacing according to a prescribed law across the grating aperture as well as of making straight and curvilinear grooves. The minimal possible spacing increment was equal to 0.2 Å [7]. Upon improvement of his ruling engine T. Harada was able to make gratings with an average groove density up to $p_0 \approx 10^4$ mm^{-1} and up to 300 mm in width and 200 mm in length [46]. At present (after T. Harada's retirement from Hitachi) the company makes only the replicas of the available master gratings.

There are reports about the fabrication of plane VLS gratings by Carl Zeiss Optronics GmbH (Germany) with GTM6 ruling engine [42]. At present the engine is at the disposal of Helmholtz-Zentrum Berlin für Materialien und Energie.

Electron-beam lithography is another technology suitable for VLS-grating fabrication. The method involves exposing a resist to an electron beam with subsequent plasma-chemical etching. The electron beam 'writes' a requisite pattern of VLS-grating lines on a resist. Upon exposure to the electron beam the resist is developed and etched away, after which the grating material is etched away from the exposed regions, thereby transferring the VLS-grating line pattern onto the grating material. The remaining protective resist is removed at the last stage. This technique was used to make the first domestic VLS grating for SXR spectral domain at the Centre for Shared Use of the MIPT (Fig. 18) [38]. The VLS-grating line pattern was made in a 100-nm thick tungsten film deposited on a plane-parallel substrate of K8 glass.

In the e-beam 'patterning' of the resist, which covers the tungsten layer, there emerges the problem of 'stitching' differ-

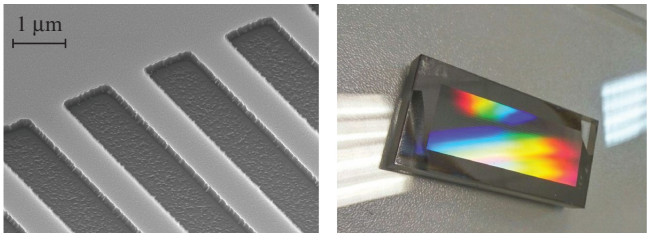

Figure 18. (a) SEM photograph of a portion of the tungsten VLS grating on a glass substrate and (b) photograph of this grating of aperture 40×16 mm.

ent portions of the lithographic pattern due to possible errors of mechanical positioning of the substrate. The problem of 'stitching' the exposure fields in a large aperture (40×16 mm in our case) is the general problem of e-beam lithography technique. When the positioning inaccuracy is comparable with the local line spacing, this may limit the spectral resolution of the VLS grating and its based spectrometer. Figure 19 provides an example of an inexact 'stitching' of this kind.

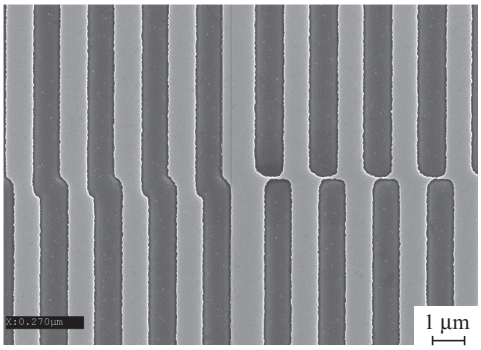

Figure 19. Example of inexact 'stitching' of exposure fields of one of the test samples of the tungsten VLS grating made by e-beam lithography technique.

Interference lithography now is one of the most production-friendly approaches to the fabrication of VLS gratings. In this case, the grating grooves are formed in the course of exposure (writing) the interference pattern of two waves on photoresist and its subsequent processing. Selecting the writing scheme that approximates the requisite spatial groove density distribution across the aperture with the interference fringe frequency distribution is a nontrivial problem. The spectral resolution of the instrument in which the grating under fabrication is planned to be used will depend on how close the approximation will be, and therefore the solution of this problem is of first importance. These problems were successfully solved in Japan in the making of VLS gratings for a flat-field spectrograph [47, 48]. For an auxiliary optical element, Koike et al. [47] employed a spherical mirror at oblique-incidence. VLS gratings made by interference lithography are commercially available (for instance, Shimadzu gratings [49]). The first domestic interference-lithographed plane VLS grating for SXR spectral domain was made at the Institute of Applied Optics using 532-nm light (Fig. 20) [40].

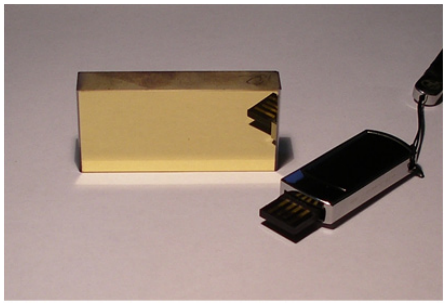

Figure 20. Photograph of a gold-coated VLS grating with an area of 55×25 mm made by interference lithography at a wavelength of 532 nm.

By now we have solved the problem of numerical design of the interference lithographic optical scheme that realises the desired spatial distribution of the interference fringe frequency over the aperture of a plane or spherical substrate (VLS grating), i.e. the frequency dependence described by the polynomial $p(w)$ (1). The solution of the problem involves control over the radius of curvature of the fringes (grating grooves). Work in this direction is being continued [50].

8. Conclusions

In this paper we endeavoured to describe two different classes of aperiodic elements for SXR optics and spectroscopy, namely, plane and concave reflection DGs with a monotonic variation of the spacing across the VLS grating aperture. They offer several advantages over 'classical' gratings of the SXR region (over DGs with equidistant grooves) and their combination with other optical elements (MMs, aspherical grazing-incidence mirrors, etc.) in one instrument opens up fresh possibilities for research.

For example, broadband normal-incidence MMs in combination with reflection VLS gratings participate in the construction of high-resolution stigmatic spectral images in the SXR region. Earlier (before the 1990s) the construction of stigmatic spectral images in the VUV was possible with spectrometers for $\lambda > 30$ nm. Developed by the time of writing this manuscript were broadband normal-incidence mirrors based on aperiodic Mo/Si structures efficient in the 12–30 nm range [39], broadband palladium-bearing MMs for the 8.9–11.2 nm range (i.e. in the wavelength range shorter than the K edge of beryllium) [51], as well as Sb/B_4C-based MMs in the 9–12 nm range [52]. Furthermore, broadband normal-incidence Mo/Be (Rh/Be) MMs possess, according to calculations, higher reflection coefficients in the 11–13 nm domain and their use will improve the construction efficiency of stigmatic spectral images in this domain, while the synthesis of broadband La/B_4C MMs will extend this domain to about 6.9 nm. Further extension of this domain towards shorter wavelengths may be related to grazing-incidence aspherical mirrors (for instance, elliptical). But even in this case, too, the benefit of depositing an aperiodic reflective multilayer coating will be significant, making it possible to increase the grazing-incidence angle and shorten the mirror length several-fold. The main achievements in this direction are yet to be made and their realisation will largely depend on the progress of technology.

In the past, special photoemulsion deposited on a thin photographic plate or film was used to record VUV and SXR spectra. At present there exists a demand in a prompt (quite often in real time) spectra processing in various experiments and measurements. This possibility is provided by modern detectors with electric readout of the signal. The advent of modern digital detectors, including backside-illuminated CCD matrices for the SXR region, called for development of flat-field SXR spectrometers and monochromators. In this case, VLS-grating spectrometer schemes offer indisputable advantages over classical diffraction grating spectrometers: the focal surface of a flat-field VLS spectrometer is perpendicular or nearly perpendicular to the rays and is well approximated by a plane, and the focal distance of a scanning VLS spectrometer/monochromator remains invariable in the scanning throughout a broad spectral range for invariable positions of the remaining elements of the scheme.

Concave VLS gratings are employed in broadband (about two octaves in width, for instance 5–20 nm, 1–5 nm) spectrometers of fixed geometry. In this spectral interval the spectral resolution is defined by the dispersion and the spatial detector resolution, and is numerically equal to about double the product of the plate scale and the CCD detector pixel size. In this case, the working width of the VLS grating (and the acceptance angle) may somewhat exceed the width of a classical DG due to aberration compensation in the working spectral range.

Recent years have seen a considerable diversification of plane VLS grating schemes, which is evident from the examples provided in this review. Plane VLS gratings operate both in converging and diverging beams. They are employed in broadband spectrographs with invariable geometry as well as in scanning spectrometer/monochromator schemes. Realised in the latter case is the remarkable scheme with immobile input and output slits (or detector) with retention of the requisite spectral resolution.

Acknowledgements. This research was supported by the Russian Science Foundation (Project No. 14-12-00506).

9. References

1. Rowland H.A. *Phil. Mag*., **13**, 469 (1882).
2. Samson J.A.R. *Techniques of Vacuum Ultraviolet Spectroscopy* (New York: Wiley, 1967).
3. Mack J.E., Stehn J.R., Edlen B. *J. Opt. Soc. Am*., **22**, 245 (1932).
4. Edlen B. *Usp. Fiz. Nauk*, **89** (3), 483 (1966).
5. Cornu M.A. *Comptes Rendus Acad. Sci*., **117**, 1032 (1893).
6. Gerasimov F.M., Yakovlev E.A., Peisakhson I.V., Koshelev B.V. *Opt. Spektrosk*., **28** (4), 790 (1970).
7. Harada T., Kita T. *Appl. Opt*., **19** (23), 3987 (1980).
8. Hettrick M.C., Bowyer S. *Appl. Opt*., **22** (24), 3921 (1983).
9. Hettrick M.C., Underwood J.H. *AIP Conf. Proc*., **147**, 237 (1986).
10. Namioka T. *J. Opt. Soc. Am*., **49** (5), 446 (1959).
11. Wadsworth F.L.O. *Astrophys. J*., **3**, 47 (1896).
12. Vishnyakov E.A., Kolesnikov A.O., Ragozin E.N., Shatokhin A.N. *Quantum Electron*., **46** (10), 953 (2016) [*Kvantovaya Elektron*., **46** (10), 953 (2016)].
13. Ragozin E.N., Vishnyakov E.A., Kolesnikov A.O., Pirozhkov A.S., Shatokhin A.N. *Aperiodicheskie elementy v optike myagkogo rentgenovskogo diapazona* (Aperiodic Elements in Soft X-Ray Optics) (Moscow: Fizmatlit, 2018).
14. Kita T., Harada T., Nakano N., Kuroda H. *Appl. Opt*., **22** (4), 512 (1983).
15. Pirozhkov A.S., Kando M., Esirkepov T.Zh., Gallegos P., Ahmed H., Ragozin E.N., Faenov A.Ya., Pikuz T.A., Kawachi T., Sagisaka A., Koga J.K., Coury M., Green J., Foster P., Brenner C., Dromey B., Symes D.R., Mori M., Kawase K., Kameshima T., Fukuda Y., Chen L., Daito I., Ogura K., Hayashi Y., Kotaki H., Kiriyama H., Okada H., Nishimori N., Imazono T., Kondo K., Kimura T., Tajima T., Daido H., Rajeev P., McKenna P., Borghesi M., Neely D., Kato Y., Bulanov S.V. *Phys. Rev. Lett*., **108**, 135004 (2012).
16. Pirozhkov A.S., Kando M., Esirkepov T.Zh., Gallegos P., Ahmed H., Ragozin E.N., Faenov A.Ya., Pikuz T.A., Kawachi T., Sagisaka A., Koga J.K., Coury M., Green J., Foster P., Brenner C., Dromey B., Symes D.R., Mori M., Kawase K., Kameshima T., Fukuda Y., Chen L., Daito I., Ogura K., Hayashi Y., Kotaki H., Kiriyama H., Okada H., Nishimori N., Imazono T., Kondo K., Kimura T., Tajima T., Daido H., Rajeev P., McKenna P., Borghesi M., Neely D., Kato Y., Bulanov S.V. *New J. Phys*., **16**, 093003 (2014).
17. Pirozhkov A.S., Esirkepov T.Zh., Pikuz T.A., Faenov A.Ya., Ogura K., Hayashi Y., Kotaki H., Ragozin E.N., Neely D., Kiriyama H., Koga J.K., Fukuda Y., Sagisaka A., Nishikino M., Imazono T., Hasegawa N., Kawachi T., Bolton P.R., Daido H., Kato Y., Kondo K., Bulanov S.V., Kando M. *Sci. Rep*., **7**, 17968 (2017).
18. Neely D., Chambers D., Danson C., et al. *AIP Conf. Proc*., **426**, 479 (1998).
19. Beiersdorfer P., Magee E.W., Träbert E., et al. *Rev. Sci. Instrum*., **75** (10), 3723 (2004).
20. Dunn J., Magee E.W., Shepherd R., et al. *Rev. Sci. Instrum*., **79**, 10E314 (2008).
21. Terauchi M., Koshiya S., Satoh F., et al. *Microsc. Microanal*., **20** (3), 692 (2014).
22. Terauchi M., Koike M., Fukushima K., Kimura A. *J. Electron Microsc*., **59** (4), 251 (2010).
23. Imazono T., Koike M., Kawachi T., et al. *Appl. Opt*., **51** (13), 2351 (2012).
24. https://www.jeol.co.jp/en/products/detail/SXES.html.
25. Hettrick M.C., Underwood J.H., Batson P.J., Eckart M.J. *Appl. Opt*., **27** (2), 200 (1988).
26. Koch J.A., MacGowan B.J., Da Silva L.B., Matthews D.L., Underwood J.H., Batson P.J., Mrowka S. *Phys. Rev. Lett*., **68** (22), 3291 (1992).
27. http://hettrickscientific.com/.
28. Underwood J.H., Gullikson E.M., Koike M., Mrowka S. *Proc. SPIE*, **3150**, 40 (1997).
29. Wang J.-J., Mao Y.E., Shi T., Chang R., Qiao S. *Chin. Phys. C*, **39** (4), 048001 (2015).
30. Du L., Du X., Wang Q., Zhong J. *Nucl. Instr. Meth. Phys. Res. A*, **877**, 65 (2018).
31. Miyake A. et al. *Proc. SPIE*, **5037**, 647 (2003).
32. Hettrick M.C., Bowyer S., Malina R.F., Martin C., Mrowka S. *Appl. Opt*., **24** (12), 1737 (1985).
33. Sirk M.M., Vallerga J.V., Finley D.S., Jelinsky P., Malina R.F. *Astrophys. J. Suppl. Ser*., **110**, 347 (1997).
34. Craig N., Abbott M., Finley D.S., Jessop H., Howell S.B., Mathioudakis M., Sommers J., Vallerga J.V., Malina R.F. *Astrophys. J. Suppl. Ser*., **113**, 131 (1997).
35. Bowyer S., Lampton M., Lewis J., Wu X., Jelinsky P., Malina R.F. *Astrophys. J. Suppl. Series*, **102**, 129 (1996).
36. https://archive.stsci.edu/euve/allsky/results.html.
37. Vishnyakov E.A., Ragozin E.N., Shatokhin A.N. *Quantum Electron*., **45** (4), 371 (2015) [*Kvantovaya Elektron*., **45** (4), 371 (2015)].
38. Vishnyakov E.A., Kolesnikov A.O., Kuzin A.A., Negrov D.V., Ragozin E.N., Sasorov P.V., Shatokhin A.N. *Quantum Electron*., **47** (1), 54 (2017) [*Kvantovaya Elektron*., **47** (1), 54 (2017)].
39. Shatokhin A.N., Kolesnikov A.O., Sasorov P.V., Vishnyakov E.A., Ragozin E.N. *Opt. Express*, **26** (15), 19009 (2018).
40. Ragozin E.N., Belokopytov A.A., Kolesnikov A.O., Muslimov E.R., Shatokhin A.N., Vishnyakov E.A. *Proc. SPIE*, **10235**, 102350L (2017).
41. Pirozhkov A.S., Ragozin E.N. *Phys. Usp*., **58** (11) 1095 (2015) [*Usp. Fiz. Nauk*, **185** (11), 1203 (2015)].
42. Fuchs O. et al. *Rev. Sci. Instrum*., **80**, 063103 (2009).
43. Warwick T., Chuang Y.-D., Voronov D.L., Padmore H.A. *J. Synchrotron Radiat*., **21**, 736 (2014).
44. Harada T., Moriyama S., Kita T. *Jpn. J. Appl. Phys*., **14**, 175 (1975).
45. Harada T., Moriyama S., Kita T., Kondo Y. *J. Jpn. Soc. Precision Eng*., **42**, 888 (1976).
46. Kita T., Harada T. *Appl. Opt*., **31** (10), 1399 (1992).
47. Koike M., Namioka T., Gullikson E., Harada Y., Ishikawa S., Imazono T., Mrowka S., Miyata N., Yanagihara M., Underwood J.H., Sano K., Ogiwara T., Yoda O., Nagai S. *Proc. SPIE*, **4146**, 163 (2000).
48. Namioka T., Koike M. *Appl. Opt*., **34** (13), 2180 (1995).

49. Ragozin E.N., Vishnyakov E.A., Kolesnikov A.O., Shatokhin A.N. Patent of the Russian Federation, No. 2659875, Certificate of Invention of 04.07.2018.
50. https://www.shimadzu.com/opt/products/dif/o-k25cur0000006zd0.html.
51. Windt D.L., Gullikson E.M. *Appl. Opt*., **54** (18), 5850 (2015).
52. Vishnyakov E.A., Kopylets I.A., Kondratenko V.V., et al. *Quantum Electron*., **48** (3), 189 (2018) [*Kvantovaya Elektron*., **48** (3), 189 (2018)].